Primary Quinone (Q_A) Binding Site of Bacterial Photosynthetic Reaction Centers: Mutations at Residue M265 Probed by FTIR Spectroscopy[†]

Todd A. Wells,[‡] Eiji Takahashi, and Colin A. Wraight*

Department of Biochemistry and Center for Biophysics and Computational Biology, University of Illinois at Urbana−Champaign, Urbana, Illinois 61801

Received October 7, 2002; Revised Manuscript Received February 4, 2003

ABSTRACT: In the primary quinone (Q_A) binding site of *Rb. sphaeroides* reaction centers (RCs), isoleucine M265 is in extensive van der Waals contact with the ubiquinone headgroup. Substitution of threonine or serine for this residue (mutants M265IT and M265IS), but not valine (mutant M265IV), lowers the redox midpoint potential of Q_A by about 100 mV (Takahashi et al. (2001) *Biochemistry 40*, 1020−1028). The unexpectedly large effect of the polar substitutions is not due to reorientation of the methoxy groups as similar redox potential changes are seen for these mutants with either ubiquinone or anthraquinone as Q_A. Using FTIR spectroscopy to compare Q_A^-/Q_A IR difference spectra for wild type and the M265 mutant RCs, we found changes in the polar mutants (M265IT and M265IS) in the quinone C═O and C═C stretching region (1600−1660 cm^{-1}) and in the semiquinone anion band (1440−1490 cm^{-1}), as well as in protein modes. Modeling the mutations into the X-ray structure of the wild-type RC indicates that the hydroxyl group of the mutant polar residues, Thr and Ser, is hydrogen bonded to the peptide C═O of Thr^{M261}. It is suggested that the mutational effect is exerted through the extended backbone region that includes Ala^{M260}, the hydrogen bonding partner to the C1 carbonyl of the quinone headgroup. The resulting structural perturbations are likely to include lengthening of the hydrogen bond between the quinone C1═O and the peptide NH of Ala^{M260}. Possible origins of the IR spectroscopic and redox potential effects are discussed.

The primary event in photosynthesis is light-driven charge separation, catalyzed by a chlorophyll-containing protein complex, the reaction center (RC)[1]. On time scales longer than a nanosecond, the charge separation in RCs from purple bacteria resides on the primary donor, P, a dimer of bacteriochlorophyll, and on the acceptor quinones. The primary quinone, Q_A, is tightly bound in a helix−loop−helix motif of the M subunit and functions as a one-electron redox species. The secondary quinone, Q_B, which is reversibly bound in a similar helix−loop of the L subunit, can be doubly reduced via Q_A^- and, with the uptake of two protons, is released as quinol and replaced by another quinone (reviewed in refs *1* and *2*). From the known structures of bacterial RCs, Q_A and Q_B are positioned symmetrically about an iron−histidine complex, and both quinones are bound by a hydrogen bond between the C4 carbonyl[2] and a histidine (*3*, *4*).

In *Rhodobacter sphaeroides*, Q_A and Q_B are both ubiquinone-10 (Q-10), and the distinct redox properties of the bound quinones, and thus the kinetic and equilibrium behavior of both electron transfers, must be imparted by specific protein−quinone interactions. Primary influences might be the polarity of the binding site, the local electrostatic potential, and accessibility to protonation. The torsional angle of the methoxy groups with respect to the quinone plane is also known to substantially modulate the redox and pK_a properties of ubiquinone and may also be important in determining the differences between Q_A and Q_B (*5*−*8*).

Apart from the hydrogen bonding histidine residue, His^{M219}, the binding site of Q_A comprises apolar side chains and backbone aspects. The headgroup is sandwiched between tryptophan M252 and isoleucine M265. Trp^{M252} is in $\pi-\pi$ interaction with Q_A and has been shown by mutagenesis to be important for the rapid reduction of Q_A and for high affinity quinone binding (*9*, *10*).

Ile^{M265} is in van der Waals contact (<4 Å) with the C3 methoxy group, the C4 carbonyl, C5, C6, and the C5′ methyl of Q_A (Figure 1). Mutation of this residue to the smaller, polar residues of serine and threonine, but not valine, caused a large drop (80−110 mV) in the midpoint potential (E_m) of Q_A (*11*, *12*). Since the same change in E_m was observed with either native Q-10 or 9,10-anthraquinone acting as Q_A, the mechanism does not involve the conformation of the methoxy substituents of ubiquinone. Thus, the mutational effect presents an opportunity for examining local protein influences on cofactor function. To gain more specific insight to

[†] This work was supported by a grant from the National Science Foundation (MCB99-05672). T.A.W. was supported by a postdoctoral traineeship from the Integrative Photosynthesis Research Training Program, a NSF IGERT grant (DBI96-02240).

* Corresponding author. E-mail: cwraight@uiuc.edu.

[‡] Present address: Department of Chemistry and Biochemistry, University of Denver, 2190 E. Iliff Avenue, Denver, CO 80208.

[1] Abbreviations: DAD, 2,3,5,6-tetramethyl-*p*-phenylenediamine; FTIR, Fourier transform infrared; LDAO, lauryl(C_{12})-dimethylamine-*N*-oxide; Q_A (Q_B), primary (secondary) quinone acceptors; Q-n, 2,3-dimethoxy-5-methyl-6-(*n*-isoprenyl)-1,4-benzoquinone; RC, reaction center; *Rb.*, *Rhodobacter*.

[2] The numbering system used here denotes ubiquinone-10 as 2,3-dimethoxy-5-methyl-6-decaisoprenyl-1,4-benzoquinone.

10.1021/bi026958j CCC: $25.00
Published on Web 03/18/2003

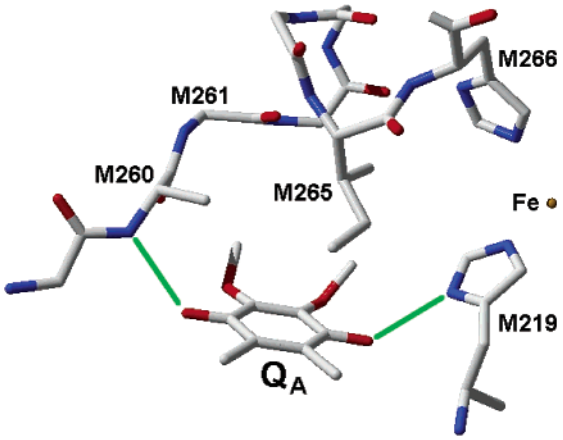

FIGURE 1: Structure near residue M265 of the Q_A binding site in wild-type RCs. Side chains are shown only for Ala^{M260}, Ile^{M265}, and His^{M266}. The hydrogen bonds to the quinone C1 and C4 carbonyl groups are shown in green. Figure drawn in SPDV 3.7b2 (*24*) and rendered in POV-Ray. Coordinates from 1AIJ for R26 RCs (*25*).

the nature of the protein−quinone interactions, we have used Fourier transform infrared spectroscopy (FTIR) to look at the vibrational features characteristic of the Q_A^-/Q_A difference spectra of the three mutant RCs, with $Ile^{M265} \rightarrow$ Ser, Thr, Val (mutants M265IS, M265IT, and M265IV), and the wild type.

MATERIALS AND METHODS

The mutagenesis procedures, growth conditions for mutant cells, as well as the RC preparation procedure, have been described previously (*12*−*14*). The mutations were obtained by in vitro mutagenesis, following the procedure of Kunkel (*15*). The parent for the expression background was the green, carotenoid-containing strain, Ga.

For FTIR sample preparation, aliquots of Ga wild type and M265 mutant RCs were partially dried on a CaF_2 window in a vacuum, then rehydrated, and covered with another CaF_2 window separated by a 6-μm spacer. On the basis of the rehydration volume, the final concentrations were approximately 300 μM RCs in 30 mM Tris buffer, pH 8.0, 0.3% LDAO, 500 μM terbutryn, 5 mM diaminodurene, and 10 mM ascorbate. Deuterated samples were rehydrated in 99% deuterium oxide (^2H_2O).

Spectra were recorded on a BioRad 575C FTIR spectrometer equipped with an MCT detector. The sample temperature was adjusted to 283 K in a Harrick transmission cell with an Automatic Temperature Controller (Harrick Scientific Corp., model ATC-30D). An 870-nm fiber-coupled, CW diode laser (Optopower Corp., model OPC-A001-870-FC/100) was used for actinic illumination. All absolute spectra are representative of ~2000 co-added interferograms, collected as an automated repetitive series of 25 dark scans followed by 25 light scans with a 5 min dark relaxation time between each set. Data were collected at 4 cm^{-1} resolution. We have followed the practices of earlier authors, especially Breton and co-workers, and have computed light-minus-dark (Q_A^--minus-Q_A) difference spectra and wild type-minus-mutant and ^1H_2O-minus-^2H_2O double difference spectra. Difference spectra were generated by subtracting the average of all dark spectra from that of the averaged light spectra for each sample. To determine double difference spectra,

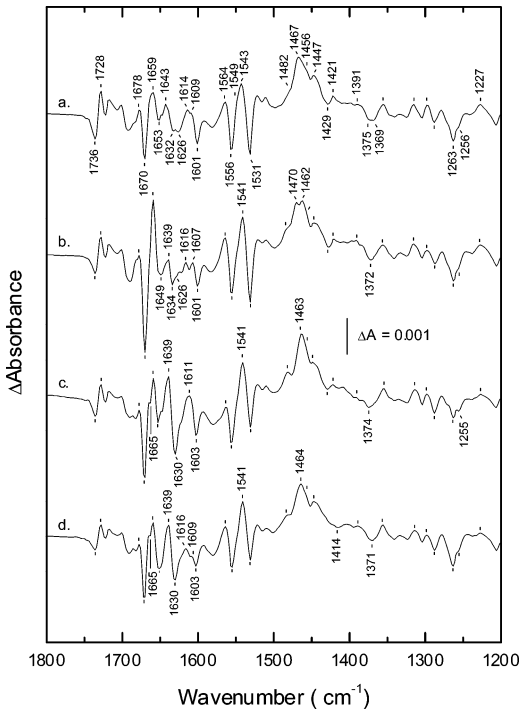

FIGURE 2: Light-induced, Q_A^--minus-Q_A, infrared absorption spectra of wild type and M265 mutant RCs from *Rb. sphaeroides*, in ^1H_2O: (a) wild-type RCs (GaWT), (b) $Ile^{M265} \rightarrow$ Val mutant RCs (M265IV), (c) $Ile^{M265} \rightarrow$ Ser mutant RCs (M265IS), and (d) $Ile^{M265} \rightarrow$ Thr mutant RCs (M265IT). Unlabeled markers in mutant spectra have the same wavenumber values as in wild type. Frequencies are given with an accuracy of ±1 cm^{-1}.

difference spectra were initially normalized on the 1263 cm^{-1} (methoxy) band, and further adjustments were then made to minimize differences in the 1300−1400 cm^{-1} region. As noted by earlier workers, changes in scaling factor by as much as 20% did not alter the main features of the double difference spectra (*16*).

RESULTS

Comparison of Wild-Type and M265IV RCs in ^1H_2O. In the light induced difference spectra (Q_A^--minus-Q_A), the bands of the ground state (with neutral quinone) are negative, while those of the photoproduct state (with anionic semiquinone) are positive. This applies to both cofactor (quinone) and protein, for which small frequency shifts in protein modes can give rise to numerous positive−negative features, especially in the so-called amide bands of the peptide backbone.

The Q_A^-/Q_A difference spectrum for Ga wild type RCs (here designated GaWT, Figure 2a) is essentially identical to those reported previously for R26 and 2.4.1 wild type (*16*−*19*). The large features at 1650−1670 cm^{-1}, which are somewhat variable, are in the amide I region (predominantly C═O stretch) of the protein and are not usually given specific interpretation. They indicate the response of the peptide bond network to changes induced by the semiquinone anion. The smaller changes throughout the region 1630−1680 cm^{-1} are also largely attributable to the amide I band.

Neutral Quinone Spectrum. The contributions of the neutral quinone to the Q_A^-/Q_A difference spectrum for M265IV mutant RCs (Figure 2b) are very similar to those

of GaWT. In particular, the characteristic band at 1601 cm^{-1}, which has been assigned to the C4 carbonyl (C4═O) in R26 and wild type RCs (*18*, *19*), is unaltered. The C1 carbonyl (C1═O) stretch, at ≈1660 cm^{-1}, is buried in the amide I band and is only extractable by isotope editing with ^{13}C and/or ^{18}O labeling (*18*, *19*).

The peak at 1626−1628 cm^{-1} has been assigned to the quinone, with mostly C═C character (*18*−*20*). In wild type RCs, this appears alongside another band at 1632−1634 cm^{-1}, of unknown origin but probably amide I, with which it forms a recognizable doublet. In the M265IV mutant, a bandshift-like difference enhances the 1634 cm^{-1} negative peak as compared to the 1626 cm^{-1} C═C stretch, but the latter is not evidently affected. Also unaltered in M26IV RCs are the negative peak at 1263 cm^{-1}, identified with the methoxy C−O−C bend, and a shoulder at 1256 cm^{-1}.

Semiquinone Anion Spectrum. More notable differences are seen in the anion band region of the semiquinone spectrum, centered at about 1465 cm^{-1} (Figure 2). In GaWT, as in other wild type strains (*8*, *17*), we observe the main peak at 1467−1468 cm^{-1}, with a shoulder at 1456 cm^{-1} that gives it a distinct asymmetric appearance. An additional shoulder[3] is seen at 1482 cm^{-1} and a small peak at 1447 cm^{-1}. A smaller peak at 1421 cm^{-1} has also been assigned to the semiquinone anion (*17*, *18*, *20*), but the quinonic contribution is, at most, only part of the observed peak.

In the valine mutant, the main peak of the anion band is split, with peaks at 1462 and 1470 cm^{-1}. The curvature on the low-frequency side indicates that the shoulder at 1456 cm^{-1} is still present, and the minor peak at 1447 cm^{-1} is still quite distinct. The shoulder at 1482 cm^{-1} is more pronounced than in GaWT.

Polar Mutants, M265IS and M265IT, in ^1H_2O. In view of the small but significant differences between GaWT and M265IV, the polar mutants, M265IT and M265IS, were compared to both (Figure 2). In the most prominent difference feature of the amide I region, at 1670(−)/1659(+) cm^{-1}, both polar mutants exhibited a distinctive notch at 1665 cm^{-1} that is absent in GaWT and M265IV RCs. In wild type-minus-mutant double difference spectra, this appears as a peak at 1666 cm^{-1} (not shown). The polar mutants also showed a substantial bandshift feature at 1639(+)/1630(−). This is at the low frequency side of the amide I band, possibly identifiable with β-structure (*21*). The well-defined feature at 1736(−)/1728(+) cm^{-1}, which is seen in all strains, is smaller in the two polar mutants.

Neutral Quinone Spectrum. In contrast to the valine mutant, both polar mutants (M265IS and M265IT, Figure 2c,d) showed a small but distinct shift to higher frequency for the C4═O stretch, and the peak is at 1603 cm^{-1} as compared to 1601 cm^{-1} in GaWT and M265IV. In wild type-minus-mutant double difference spectra, this shows as a negative peak at 1599 cm^{-1} and a positive peak at 1605 cm^{-1} (see Figure 5 for spectra in ^2H_2O).

In both polar mutants, an apparent bandshift generates a pronounced negative peak at 1630 cm^{-1} that obscures the C═C stretch at 1626 cm^{-1}, and it is not clear if this may have shifted at all. The peak position of the methoxy band at 1263 cm^{-1} is unchanged in the polar mutants, but in M265IS the amplitude is significantly less, and a distinct peak is seen at 1255 cm^{-1}.

Semiquinone Anion Spectrum. Unlike in the valine mutant, in the polar mutants the semiquinone anion band is not split but shows a single, main peak that is shifted down by 3−4 cm^{-1}, to 1463 cm^{-1} for M265IS and 1464 cm^{-1} for M265IT (Figure 2c,d). The main peak in the polar mutants is more symmetrical than in GaWT, and the shoulder at 1455−1457 cm^{-1} is barely discernible. Both polar mutants exhibit a distinct peak at 1482 cm^{-1}, rather than a shoulder.

The trough and peak at 1429 and 1421 cm^{-1} are less pronounced in M265IS and are completely flattened out in M265IT RCs. The double difference spectra between M265IT and either GaWT or M265IV RCs suggest that the missing feature is a negative band at 1429 cm^{-1}.

1500−1600 cm^{-1} Region. This region of the IR spectrum is dominated by the amide II band (coupled C−N and N−H modes) that, like the amide I band, can reflect global influences on the protein backbone. In all RCs, there is a significant and characteristic feature between 1565 and 1530 cm^{-1}, with few obvious differences between the strains. In GaWT, positive peaks are at 1564 and 1543 cm^{-1}, with a shoulder at 1549 cm^{-1}, and negative peaks are at 1556 and 1531 cm^{-1}. The 1549 cm^{-1} shoulder is missing in all mutant strains, and the center peak is shifted down by 2 cm^{-1}. In M265IS mutant RCs, there is significant positive amplitude missing at ≈1570 cm^{-1}.

1200−1400 cm^{-1} Region. Many small amplitude signals are seen throughout the low-frequency region of the spectrum, between 1200 and 1400 cm^{-1}, most of which are unaffected in any of the mutants. However, some subtle differences in band shapes and frequencies are seen, most notably at 1385−1400 cm^{-1} and 1365−1375 cm^{-1}. All mutant RCs show a single negative peak at ≈1373 cm^{-1}, whereas GaWT has two, at 1369 and 1375 cm^{-1}. In double difference spectra between GaWT and the mutant RCs, the missing signal is evident at 1368 cm^{-1} (not shown, but see Figure 5 for double difference spectra in ^2H_2O). Several small positive peaks are seen in all strains, at 1383, 1391, and 1398 cm^{-1}, but the serine mutant is missing a broad positive band underlying these and centered at ≈1395 cm^{-1}.

IR Spectra in ^2H_2O. Infrared spectra in ^2H_2O can sometimes simplify and sharpen responses in the amide I region, by shifting the intense HOH bend absorbance from ≈1640 to ≈1210 cm^{-1}. They may also reveal frequency shifts in hydrogen bonded vibrations because of the greater mass of ^2H. This offers some opportunity for identifying vibrational modes containing N, O, and S. The Q_A^-/Q_A difference spectra for all RC types in ^2H_2O are shown in Figure 3.

For all RC types, the major differences in ^2H_2O versus ^1H_2O are essentially as reported previously for the carotenoidless strain, R26 (*22*), and the wild type strain, 2.4.1 (*16*). These include (i) a small downshift in the peak at 1728 cm^{-1}, (ii) a larger negative peak at ≈1670 cm^{-1}, (iii) a pronounced peak at 1614 cm^{-1}, (iv) a large apparent increase in the positive band at 1562 cm^{-1} and decrease in the negative peak at 1554 cm^{-1}, (v) a more pronounced shoulder at 1482 cm^{-1}, and (vi) significant shifts of components on the low frequency side of the semiquinone anion band, especially the minor peak at 1447 cm^{-1} and the shoulder at 1456 cm^{-1}.

[3] In some reports the signal at 1482−1484 cm^{-1} is a distinct peak, depending on the intensity of an underlying negative band (neutral Q_A-associated) (*19*).

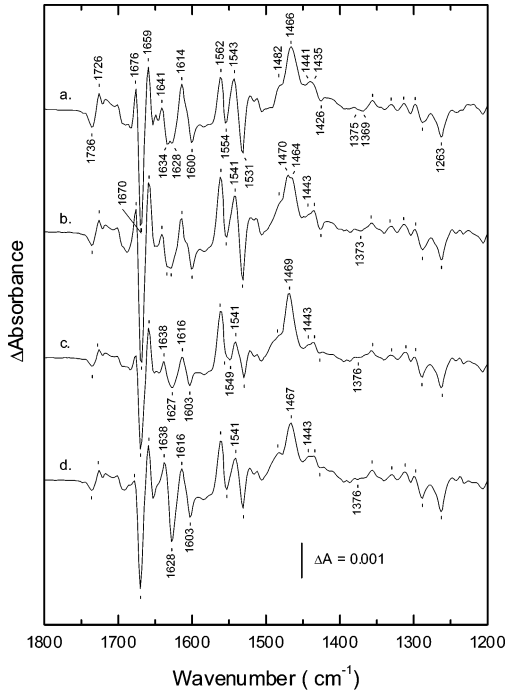

FIGURE 3: Light-induced, Q_A^--minus-Q_A, infrared absorption spectra of wild type and M265 mutant RCs from *Rb. sphaeroides*, in ^2H_2O: (a) wild-type RCs (GaWT), (b) M265IV mutant RCs, (c) M265IS mutant RCs, and (d) M265IT mutant RCs. Unlabeled markers in mutant spectra have the same wavenumber values as in wild type. Frequencies are given with an accuracy of ±1 cm^{-1}.

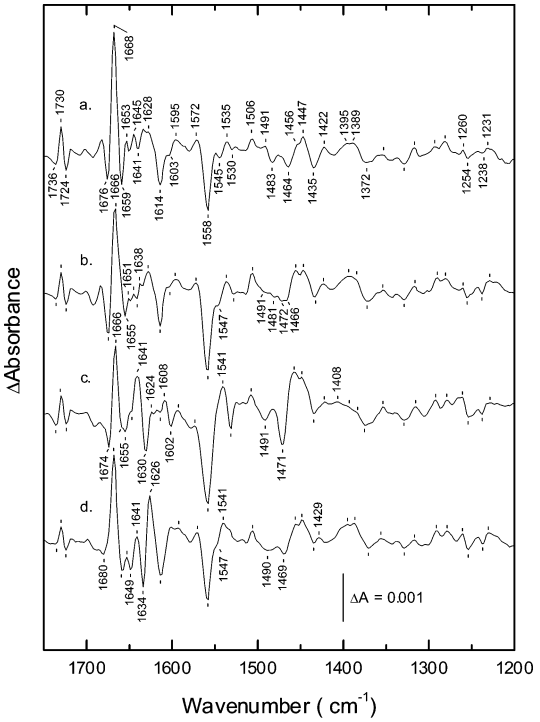

FIGURE 4: ^1H_2O-minus-^2H_2O double difference infrared spectra of wild type and M265 mutant RCs: (a) wild-type RCs (GaWT), (b) M265IV mutant RCs, (c) M265IS mutant RCs, and (d) M265IT mutant RCs. Unlabeled markers in mutant spectra have the same wavenumber values as in wild type. Frequencies are given with an accuracy of ±1 cm^{-1}.

In addition to these previously reported effects, we observed the suppression of the shoulder or small peak on the low-frequency side of the methoxy signal at 1263 cm^{-1}, seen at ≈1255 cm^{-1} in all strains in ^1H_2O. This appears at 1260(+)/1254(−) cm^{-1} in the ^1H_2O-minus-^2H_2O double difference spectra (Figure 4, see below). A similar shift is evident in the spectra of Breton and Nabedryk (*22*).

Neutral Quinone Spectrum. In wild type RCs, the neutral quinone modes at 1628 and 1601 cm^{-1} have been reported to be unaffected by ^2H_2O exchange (*16*, *22*). In fact, a very small (<1 cm^{-1}) downshift may occur in all cases here. All strains show an increase or sharpening of a positive band at 1614 cm^{-1}. In the polar mutants, the bandshift responsible for the 1630 cm^{-1} single negative peak in ^1H_2O downshifts to 1628 cm^{-1} in ^2H_2O, completely obscuring the C═C stretch. However, the double peaks in GaWT, at 1634 and 1628 cm^{-1}, are not detectably affected. In M265IV RCs, a double peak appearance at 1634 and 1628 cm^{-1} is recovered in ^2H_2O because of a shift in the overlying feature at 1634 cm^{-1} (in ^1H_2O).

Semiquinone Anion Spectrum. In both GaWT and M265IV RCs, the main semiquinone anion peak sharpens in ^2H_2O, but the double peak in M265IV remains intact. The peak in GaWT appears to downshift slightly, to 1466 cm^{-1}, and becomes more symmetrical. The twin peaks in M265IV move closer together with an upshift of the 1462 cm^{-1} peak to 1464 cm^{-1}, but there is no change in the higher frequency peak at 1470 cm^{-1}.

For the polar mutants, the single main peak (at ≈1464 cm^{-1} in ^1H_2O) is significantly upshifted in ^2H_2O, by 3 cm^{-1} for M265IT and 5−6 cm^{-1} for M265IS. In all strains, the shoulder at 1456 cm^{-1} disappears, and the minor peak at 1447 cm^{-1} downshifts substantially in ^2H_2O, with the effect that the main anion band sharpens.

Double Difference Spectra between ^1H_2O and ^2H_2O. The spectral trends in ^2H_2O, especially the insignificant frequency shift of the 1601/1603 cm^{-1} band and the substantial shifts in the low-frequency components of the anion band, are very obvious in the ^1H_2O-minus-^2H_2O double difference spectra (Figure 4). The overall spectrum is similar in all strains, with the most dominant features localized in the amide I and II bands, at ≈1668(+) and 1558(−) cm^{-1}, and a negative peak at 1614 cm^{-1}. However, significant differences between strains with apolar and polar residues at M265 are seen in the region of 1645−1625 cm^{-1}, where the polar mutants exhibit a distinct bandshift-like feature.

The ^1H_2O-minus-^2H_2O double difference spectra make clear the lack of any significant shift in the C4═O stretch frequency, although the small perturbation seen at 1602/1595 cm^{-1}, in GaWT and M265IS RCs, may result from the slight downshift noted above. The more prominent peak seen at 1608 cm^{-1} in M265IS RCs is not related to the carbonyl absorbance and indicates a shift in a small positive band in this region, which may partially cancel the negative peak at ≈1614 cm^{-1}.

In the semiquinone anion band, the ^1H_2O-minus-^2H_2O double difference spectra of all strains show a positive, double-peaked feature at 1456−1447 cm^{-1} that corresponds to ^2H_2O-induced shifts at the low-frequency side of the main peak. About half of this intensity appears at 1435 cm^{-1}, but the rest seems to shift up to higher frequency, in the range of 1464−1472 cm^{-1}, depending on strain. The magnitude of this component is significantly greater in M265IS, as

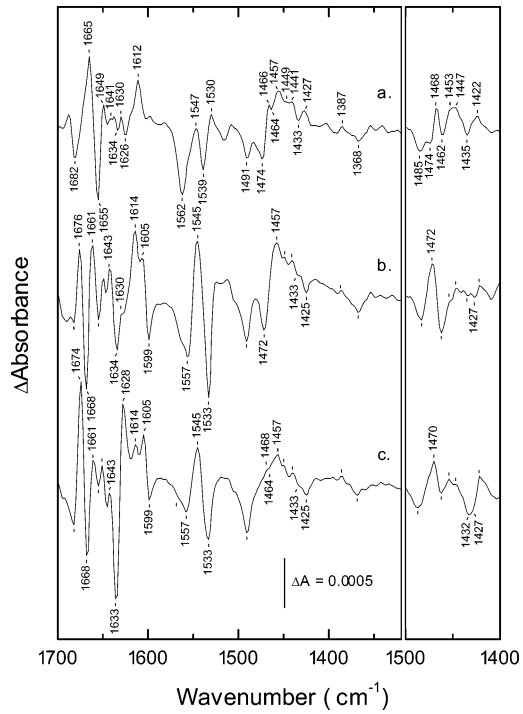

FIGURE 5: Double difference infrared spectra between GaWT wild type and M265 mutant RCs: (a) GaWT-minus-M265IV, (b) GaWT-minus-M265IS, and (c) GaWT-minus-M265IT. Main panel (left): double difference spectra in ^2H_2O, in the range of 1325−1700 cm^{-1}. Side panel (right): double difference spectra in ^1H_2O for the semiquinone anion region, 1400−1500 cm^{-1}. Unlabeled markers in lines b and c have the same wavenumber values as in line a.

expected from the substantial peak shift seen in the Q_A^-/Q_A difference spectrum.

Also evident in all strains is the downshift of a band at 1506 cm^{-1}. This is seen to move to ≈1490 cm^{-1} in the M265IS and M265IT mutants. However, in GaWT and M265IV RCs, the location of this band in ^2H_2O is obscured by the simultaneous movement of another band at about 1485 cm^{-1}. In GaWT, this is seen as a negative peak at 1483 cm^{-1} and a positive peak at 1491 cm^{-1}. This seems to correspond to an upshift of the negative band, described by Gerwert and co-workers, that is responsible for masking the minor peak of the semiquinone signal at 1482−1484 cm^{-1} in ^1H_2O (*19*). In M265IV mutant RCs, the downshift of the 1506 cm^{-1} band and the upshift of the 1485 cm^{-1} band largely cancel in the region of ≈1490 cm^{-1}. However, the negative band is quite prominent in double difference spectra between GaWT and mutant strains, both in ^1H_2O (peak at 1485 cm^{-1}, see side panel in Figure 5) and in ^2H_2O (peak at 1491 cm^{-1}, see below and main panel of Figure 5).

In all strains except M265IS, a substantial downshift is also seen for a broad band centered at about 1395 cm^{-1} in ^1H_2O and 1370 cm^{-1} in ^2H_2O. In M265IS, the intensity in ^1H_2O is more spread out and peaks at ≈1408 cm^{-1}.

Double Difference Spectra between Strains. For relatively conservative mutations, comparisons between IR responses can often be highlighted by double difference spectra between strains, and the sharpening of the anion band of the Q_A^-/Q_A difference spectrum, in ^2H_2O, is also useful when comparing different RCs. Figure 5 shows the double difference spectra between GaWT and the three mutants, in ^2H_2O (main panel); the semiquinone region in ^1H_2O is shown in the side panel.

In ^2H_2O, comparison of Figures 3 and 5 (main panel) shows the following: The upshift of the 1601 cm^{-1} band to 1603 cm^{-1} in the polar mutants gives rise to a clear difference feature at 1605−1599 cm^{-1} in the GaWT-minus-polar mutant double difference spectrum (Figure 5b,c), which is completely absent in the GaWT-minus-M265IV spectrum (Figure 5a). Compared to GaWT and the M265IV mutant, both polar mutants exhibit a slight shift in the main amide I peak near 1670 cm^{-1}, which results in a bandshift feature at 1676(+)/1668(−) cm^{-1} seen only in the wild type-minus-polar mutant double difference spectrum. This is accompanied by equivalent, small frequency differences in the amide II bands of M265IS and M265IT (at 1557(−)/1545(+) cm^{-1}). The polar mutant RCs also show a significantly larger negative peak at 1634 cm^{-1}, and in M265IT there is also a large positive peak at 1628 cm^{-1}. Increased amplitude is seen at 1612−1614 cm^{-1} in all mutants but especially in M265IS.

In the semiquinone anion band, the double difference spectrum versus GaWT is complex, but the essential features of the mutant spectra are clear. The twin peaks of the main band in M265IV give rise to a negative peak at 1474 cm^{-1}, a positive peak at 1466 cm^{-1}, and a small dip at 1464 cm^{-1} (Figure 5a). A second peak at 1457 cm^{-1} marks the top of a broad positive feature, indicative of significant intensity differences extending to 1420 cm^{-1}. In M265IS, the main peak is single, and the double difference spectrum versus GaWT shows a negative peak at 1472 cm^{-1} and a positive peak at 1457 cm^{-1} (Figure 5b). As for M265IV, the positive peak is the maximum of a broad feature at the low-frequency side of the anion band in ^1H_2O. For M265IT RCs, the main peak almost coincides with that of GaWT and the double difference spectrum versus GaWT is a broad positive band, peaking at 1457 cm^{-1}, reflecting the same main peak frequency and similar shape of the anion band in the two strains in ^2H_2O (Figure 5c). A broad positive difference is also seen, as for the other mutants.

Some of these features are even more evident in ^1H_2O, such as the wider splitting of the anion peak in M265IV mutant RCs, which produces a sharp dip at 1462 cm^{-1} (Figure 5a, side panel). Also, the distinct peak frequencies for GaWT and M265IT in ^1H_2O give rise to a well-structured difference at 1470/1462 cm^{-1}. The flattening out of the trough at 1429 cm^{-1} in the Q_A^-/Q_A difference spectra of the polar mutants, especially M265IT (Figure 2c,d), is seen as a progressive contribution at 1427 cm^{-1} in the double difference spectrum (Figure 5b,c, side panel).

A striking feature in the wild type-minus-mutant double difference spectra in ^2H_2O is the negative peak at 1491 cm^{-1}, present in all cases but largest for M265IS and M265IT (Figure 5, main panel). This indicates a negative band in GaWT that is much diminished in M265IV and missing in the polar mutants. As discussed above, a similar negative peak is seen at 1485 cm^{-1} in ^1H_2O (see side panel of Figure 5).

DISCUSSION

We have described here the results of an FTIR study on three mutants of the Q_A binding site, with residue M265 changed from isoleucine to valine, threonine, and serine. The functional consequences of these mutations place the two polar substitutions together, with a surprisingly large decrease in the E_m of Q_A (*12*). The FTIR results also ally the two

polar mutants, with similar alterations in both the neutral quinone and the semiquinone anion bands. To discuss the implications of the IR spectra for understanding the functional behavior, we first consider the possible structural consequences of the M265 mutations.

Structural Consequences of the M265 Mutations. The large effect that polar replacement of Ile^{M265} has on the E_m of Q_A ($\Delta E_m \approx -100$ mV) is seen for both native ubiquinone-10 and anthraquinone as Q_A (*12*). Thus, it is not due to the methoxy group orientation, which can be a significant source of variation in redox and acid−base properties of methoxy quinones (*5*, *7*, *8*). Instead, it must arise from nonbonded interactions with the environment.

The serine and threonine mutants, M265IS and M265IT, both manifest a distinct upshift in the 1601 cm^{-1} band in the IR spectrum, associated with the C4═O carbonyl stretch. Thus, in accounting for the marked shift in E_m of Q_A in these polar mutants, we previously focused on the potential for direct interaction between the amino acid hydroxyl oxygen and the C4 or O4 region of the quinone Q_A (*12*). However, a rotamer search around the $C_\alpha-C_\beta$ bond of serine or threonine at M265 revealed no strong interactions between the side chain O_γ and either the quinone or the nearby histidine residue (M219) that hydrogen bonds to the C4 carbonyl.

Instead, rotation of the polar side chain can place the hydroxyl group in excellent position for a strong hydrogen bonding interaction with at least the peptide C═O of Thr^{M261} (Figure 6). The minimum distance is about 2.5 Å, and the hydrogen bond angle is almost ideal without further structural adjustment, which indicates that a very strong hydrogen bond can be formed here. Using GROMOS96, implemented in Swiss PDB Viewer (SPDV v. 3.7b2) (*23*, *24*), a preliminary energy minimization was carried out on the loop and short helix comprising the Q_A binding site (residues M259−265), for the GaWT and M265 mutants, with the complete reaction center PDB file 1AIJ for the starting structure (*25*). The quinone configuration was fixed. Similar results were obtained using 1PCR (*26*) and 1K6L (*27*).

The wild type (isoleucine) and valine mutant adopted almost identical conformations of the $C_\alpha-C_\beta$ bond that were also very similar to the starting structure (Figure 6). The favored rotamer directs the side chain away from the extended backbone strand of residues M258−262, which includes the peptide NH of alanine M260, the hydrogen bond donor to the C1 carbonyl of Q_A. In contrast, the polar mutants adopt configurations in which the OH group is directed toward this segment. Two rotamer minima were found for both the threonine and the serine mutants. In one, the OH is roughly midway between the methyl group of Ala^{M260} and the peptide C═O of M261 (Figure 6a). Although this allows the shorter hydrogen bond (approximately 2.9 Å), the side chain conformation is substantially eclipsed relative to the backbone, as well as experiencing some van der Waals conflict between O_γ and the methyl group of M260. In the alternative rotamer (Figure 6b), the OH group is involved in three, longer hydrogen bonds (3.0−3.3 Å)—as a donor to two peptide C═O groups (M261 and M262) and as an acceptor from $N_\delta H$ of histidine M266 (Figure 6b). In the case of threonine, this very favorable situation may be partially offset by steric conflict between the γ-methyl and the methyl of M260 (approximately 3.6 Å).

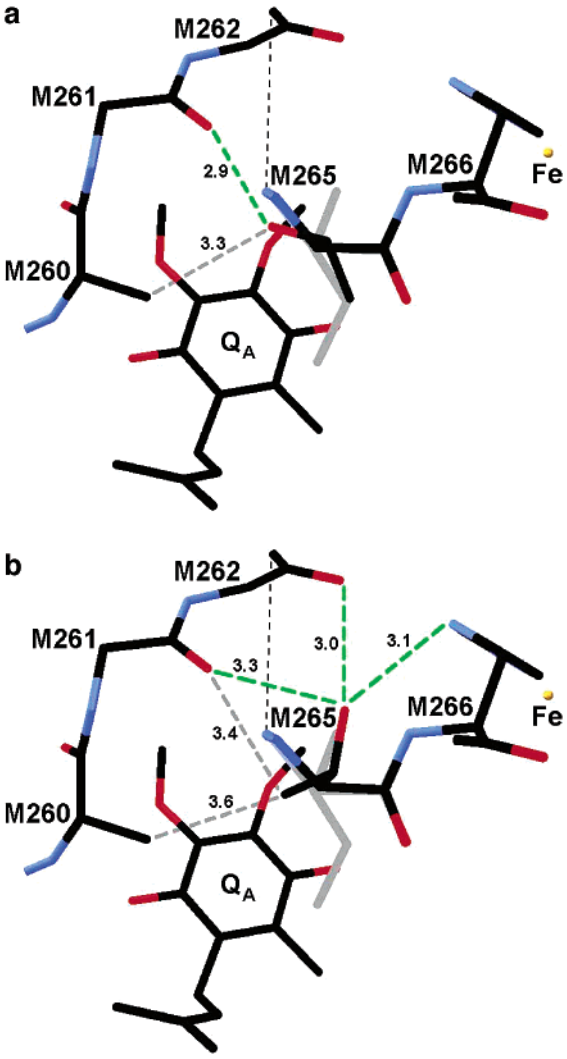

FIGURE 6: Comparison of probable rotamers for wild type and $Ile^{M265} \rightarrow$ Thr mutant RCs, looking straight down from C_α to C_β of the isoleucine side chain. (a) GaWT vs M265IT, rotamer 1 (χ (N-C_α-C_β-O_γ) $\approx -43°$). (b) GaWT vs M265IT, rotamer 2 ($\chi \approx +44°$). The side chain of the native residue, Ile^{M265}, is shown in gray. The side chain of the mutant residue, Thr^{M265}, is shown in black. Hydrogen bonds to Thr^{M265} are shown in green and van der Waals contacts in gray, with distances given in Å. The hydrogen bonding partners to Thr^{M265} in M265IT are the peptide oxygens of residues M261 and M262 and the $N_\delta H$ of His^{M266}. To simplify the diagram, residues M263−264 are omitted, as indicated by the thin, black, dotted line. The structures were determined after energy minimization on the segment M259−M265, with the full reaction center structure of PDB file 1AIJ (*25*), using GROMOS96, implemented in SPDV 3.7b2.

For serine at M265, the two favored rotamers place the OH group in almost identical positions to the OH of threonine, with the same number of hydrogen bonds. For both the serine and the threonine mutant, the energy minimization showed the two rotamers to be closely equivalent local minima, and a more sophisticated exploration of the energy landscape will be needed to decide which rotamer is actually preferred. However, in all of the local rotamer minima of the two polar mutants, contact between the M265 side chain and the peptide O of M261 and methyl of M260 pushes the M258−261 strand away. This is best conveyed by the distance between the C_β of M265 and the C_β (methyl) of Ala^{M260}. In GaWT and M265IV RCs this is 3.85 Å. In

the polar mutants the distance increases to 4.2−4.6 Å, depending on rotamer. This occurs mostly by twisting the ϕ, ψ angles of M260 and M265, which largely localizes the disturbance to these two residues (the displacement of the M265 C_β is seen in comparison of the outlines of Ile (gray) and Thr (black) in Figure 6). However, the hydrogen bond between the peptide NH of Ala^{M260} and the C1═O of Q_A lengthens by up to 0.05 Å in M265IS and 0.10 Å in M265IT.

Hydrogen bonding to the semiquinone anion is likely to be of crucial importance in setting the redox potential of the quinone, which is determined by the relative stability of the oxidized and reduced species. The IR frequency (1660 cm^{-1}) of the C1═O carbonyl stretch indicates that this group is very weakly hydrogen bonded in the oxidized state. This is consistent with studies with synthetic analogues for Q_A, which showed that the carbonyl contribution to the binding affinity is satisfied by a single carbonyl group (*28*, *29*). In contrast, ENDOR studies on the Q_A^- semiquinone suggest that both oxygens are well hydrogen bonded, albeit somewhat asymmetrically (*30*). Lengthening the hydrogen bond to C1═O will therefore destabilize the semiquinone more than the quinone, resulting in a lower midpoint potential.

On the basis of this analysis, we suggest that the serine mutant has a smaller effect on the E_m of Q_A because of the less extensive distortion of the hydrogen bond to C1═O, as indicated by the energy minimization. Some additional effect may also be due to the smaller side chain volume of serine as compared to threonine, and any effect of the side chain O−H dipole could also be different if the preferred rotamer is different, but in any case, the difference between E_m values of the two polar mutants is rather small (20−30 mV).

Q_A Neutral Quinone Spectrum. From studies with ^{18}O and ^{13}C labeled quinones, there is general agreement on the assignments of the quinone and semiquinone FTIR bands of Q_A^-/Q_A (*17*−*20*). Modes dominated by the C═O stretches of the two carbonyl groups in the neutral quinone are found at 1660 (C1═O) and 1601 cm^{-1} (C4═O). The C═C stretch (mixed with some C═O character) is seen at 1626−1628 cm^{-1}.

The C4 carbonyl frequency (1601 cm^{-1}) is extremely far shifted from the C═O positions in solution (1650 or 1665 cm^{-1} (*8*, *31*)), and this has been suggested to reflect a strong hydrogen bond to His^{M219} (*18*). De Groot has attempted to show the feasibility of this explanation (*32*), but it is not very persuasive and is not readily consistent with the negligible response to ^2H_2O exchange. Breton et al. (*16*) suggested that the hydrogen donor (His^{M219}) proton did not exchange but also reported that the semiquinone C═O modes did shift in ^2H_2O—as we also find. Furthermore, ENDOR studies on the semiquinone show exchange of the hydrogen bond donors ($N_\delta H$ of His^{M219} and NH of Ala^{M260}) to Q_A^- on time scales of a few minutes and 1−2 h (*30*, *33*)—both sufficiently rapid to allow significant or even complete exchange in the time of an FTIR experiment. Thus, this explanation for the extreme downshift of the C4 carbonyl frequency is hard to maintain. An alternative may be $\pi-\pi$ interaction between the quinone and tryptophan M252 (*12*), which overlap significantly.

Residue M265 lies against one face of the quinone ring, opposite Trp^{M252}. When Ile^{M265} is replaced by a polar, hydroxylated residue, a small but distinct upshift in frequency is seen for the carbonyl stretch associated with the C4 carbonyl, at 1601 cm^{-1}. This might be consistent with (i) a weakening of the hydrogen bond between C4═O and His^{M219}, (ii) an electrochromic effect arising from the hydroxyl partial charges, or (iii) an alteration in the $\pi-\pi$ interaction between quinone and Trp^{M252}. These have been discussed before in the context of possible mechanisms for lowering the E_m of Q_A (*12*). However, we now believe that the primary effect of the hydroxyl-containing side chain mutants is via the backbone configuration of the binding site.

In the structural scenario described above, it is suggested that the hydroxyl group of the mutant polar residues, Thr and Ser, is hydrogen bonded to the peptide C═O of Thr^{M261} and that the mutational effect is exerted through the loop that includes Ala^{M260}, the hydrogen bond donor to the C1 carbonyl of the quinone headgroup. The resulting structural perturbations are likely to include a displacement of the hydrogen bond between the peptide NH of Ala^{M260} and the C1═O. On this basis, the major IR spectroscopic effect might be expected on the C1═O stretch band at 1660 cm^{-1}, but it is effectively obscured by responses in the amide I band, and isotope editing with ^{13}C-labeled quinone will be needed to extract this. However, the stretch frequency of this group (1660 cm^{-1}) is very close to that expected for a free (non-hydrogen bonded) carbonyl, so the effect of the mutations on the neutral quinone spectrum may be slight. The more critical result is likely to be the effect on the semiquinone spectrum, which, although complex and more difficult to interpret, is evidently affected by the mutations (see below).

The small shift in the C4 carbonyl stretch seen in the M265IS and M265IT mutant RCs (from 1601 to 1603 cm^{-1}) could reflect a secondary influence of repositioning of the quinone headgroup. Breton et al. (*34*) found that tailless benzoquinones, including methyl-Q-0, have significantly (6−8 cm^{-1}) upshifted C4 carbonyl frequencies relative to isoprenyl Q-n, while dimethylnaphthoquinone has the same band position as prenylated vitamin K_1. This indicates that the isoprene chain exerts some positional constraint on the binding of the ubiquinone headgroup, in contrast to a rigid naphthoquinone headgroup of almost identical size. This is entirely consistent with the effect of the tail and other C6 substitutions on the binding affinities of ubiquinones (*6*, *35*). The upshift in the C4═O frequency in tailless ubiquinones can include contributions from reorientation of the methoxy substituents when the constraint is removed (*8*). In the polar M265 mutants, strains in the binding site may force (or allow) the quinone headgroup into a configuration approaching that naturally adopted by the tailless quinones.

Q_A^- Semiquinone Anion Band. Peak assignments in the Q_A^- spectrum have been made with less certainty than for the neutral quinone. The coupling of C═C and C═O modes is strong, the contributions in vivo are distinctly different from those in solution, and the in vivo spectrum appears to be at least somewhat sensitive to sample preparation, including the degree of hydration (*19*). At the present time, the analysis of Breton and Nabedryk (*20*) seems most consistent. In the wild type, the main peak is at 1467−1468 cm^{-1} with a shoulder at 1456−1457 cm^{-1} and a smaller peak at 1447 cm^{-1}. All these bands are identified as having significant contributions from both C1═O and C4═O. The shoulder or small peak at 1482−1484 cm^{-1} (see footnote 3) and the minor peak at 1420−1422 cm^{-1} are assigned predominantly C═C character (*20*).

Main Peak. The M265 mutants all manifest significant differences in the anion band, the most striking of which is the appearance of a split main peak in M265IV. However, the average frequency of the two M265IV peaks (1466 cm^{-1}) is little changed from that of the wild type. In ^2H_2O, the lower frequency peak in M265IV shifts up slightly, while the 1470 cm^{-1} peak is unaffected. The single peak in GaWT shifts down by no more than 1 cm^{-1} in ^2H_2O. In contrast, the main peak of the two polar mutants is at 3−4 cm^{-1} lower frequency—1463 cm^{-1} in M265IS and 1464 cm^{-1} in M265IT—and both shift significantly to higher frequency in ^2H_2O.

The unusual splitting of the M265IV semiquinone anion band is not accompanied by significant change in either the E_m of Q_A (*12*) or the C4═O frequency of the quinone. Although there is no necessary correlation between IR frequency shifts and redox potential, or between the IR frequencies for the quinone and semiquinone states, this might indicate that the spectral response is nonquinonic in origin. Other group frequencies expected in the region of the anion band include deformation modes of methyl and methylene groups, $\delta_{asym}(CH_3)$ and $\delta(CH_2)$, and the main band of the tryptophan spectrum (a mixed C−H, C−C, C−N mode) (*36*, *37*). The number and location of amino acid side chain methyl groups is different in the various M265 mutants, but it seems unlikely that these could be sufficiently perturbed by the semiquinone anion to appear in the light-minus-dark difference spectrum. Furthermore, in wild type RCs, uniform ^{13}C and ^{18}O labeling, which moves the entire spectrum by about 60 cm^{-1}, shows that the outline of the semiquinone anion band in the isotopic double difference spectrum is very similar to that in a Q_A^-/Q_A single difference spectrum (*17*). The spectral region cleared out by such labeling is almost featureless, with no distinctive candidates for protein group frequencies (*17*).

Thus, the distinct possibility remains that the peak splitting in M265IV RCs is a genuine quinone response, unique to this mutant. We have no adequate explanation for this, except to note that no assignment to the methoxy methyl groups of the quinone has been made in any in vivo Q^-/Q difference spectrum so far, and both symmetric and asymmetric CH_3 deformation modes of the methoxy group are expected to lie in this region—the asymmetric mode being upshifted by the electronegative oxygen atom (*36*, *38*). The intensity of any of these deformation modes is normally small, and it must be remembered that the spectra seen here are the result of light-induced changes in absorbance. Nevertheless, loss of the δ-carbon of the isoleucine side chain removes the most intimate of the van der Waals interactions between M265 and quinone, especially with the 3-methoxy substituent, and the minimum energy conformation of the valine substitution does not compensate for this. Thus, some movement of the quinone may be possible. In the polar mutants, the backbone movements and preferred conformations position the side chain to partially occupy the volume over the quinone face and recontact the 3-methoxy group.

It is noteworthy that in ^1H_2O the average peak position of the M265IV mutant is almost unchanged from that of the GaWT, in contrast to the polar mutants, where the peak is shifted down by about 4 cm^{-1}. It is tempting to correlate this with the effect of the mutations on the E_m of Q_A, which is unaffected in M265IV but lowered in the polar mutants. However, at the present time, the semiquinone spectrum is not sufficiently well-understood to pursue this.

Side Bands. Apart from the split peak in M265IV, the bulk of the semiquinone anion band behavior can be accounted for by three closely positioned semiquinone modes, with peak positions determined by resonance and by the environment. These include the main peak, the shoulder at 1456 cm^{-1}, and the minor peak at 1447 cm^{-1} (frequencies in ^1H_2O). The shoulder at 1456 cm^{-1} is less obvious in the M265 mutant RCs because of greater overlap with the main peak, but its continuing presence in all strains is revealed in the ^1H_2O-minus-^2H_2O double difference spectra (Figure 4), which show it to be of similar amplitude to the peak at 1447 cm^{-1}.

It is particularly striking that the position of the main peak of the anion band is essentially unaffected by ^2H_2O in GaWT and M265IV but is significantly upshifted in ^2H_2O for both polar mutants, to 1469 cm^{-1} in M265IS and 1467 cm^{-1} in M265IT. In all strains, ^2H_2O causes a substantial loss of amplitude at the low frequency side of the main band, which thereby apparently sharpens. In the case of M265IT, it could be argued that the 3−4 cm^{-1} peak shift to higher frequency is only apparent and is due to shaping effects of downshifts on both the low and the high frequency side of the band, but this is clearly not the case for M265IS where the main peak shifts by 5−6 cm^{-1}. This is not the normal response to $^1H/^2H$ exchange at a hydrogen bonded stretch mode, which would be expected to shift to lower frequency, if at all. In fact, the observed upshifts in peak position largely arise from transfer of intensity from the low-frequency sidebands at 1456 and/or 1447 cm^{-1}.

The ^1H_2O-minus-^2H_2O double difference spectra show that the effect in ^2H_2O is a simultaneous upshift in the 1456 cm^{-1} band and a downshift in the 1447 cm^{-1} band[4] (Figure 4). This unexpected response could arise from decoupling of two nearly resonant modes, with one shifting to lower frequency because of isotopic substitution and the other shifting up toward its intrinsic frequency. From the double difference spectra, the 1456 cm^{-1} band shifts variously to 1464 cm^{-1} in GaWT, 1466 cm^{-1} in M265IV, 1471 cm^{-1} in M265IS, and 1469 cm^{-1} in M265IT. The 1447 cm^{-1} band downshifts fairly uniformly to 1435 cm^{-1} in all strains.

Brudler et al. (*19*) have described the 1456 cm^{-1} feature in R26 RCs as insensitive to ^{13}C-labeling at C_1, C_4, C_5, or C_6, but their data actually show that at least a significant contribution at this frequency is affected by label at the C_4 position. Breton also found it to respond to ^{13}C-labeling at C_4 (*18*), as well as to uniform ^{13}C labeling and to ^{18}O exchange at the carbonyls (*17*). Thus, the 1456 cm^{-1} band may include contributions from the C4═O stretch mode.

On the basis of ^{13}C and ^{18}O isotope shifts, Breton and Nabedryk have assigned significant C4═O content to the 1447 cm^{-1} peak (*18*, *20*), whereas Brudler et al. (*19*) proposed this signal to be a predominantly C═C mode. It should be noted that part of the basis for the assignment of Breton and co-workers was that this peak shifts in ^2H_2O. In their original report on Q_A^-/Q_A IR spectra in ^2H_2O, Breton and Nabedryk (*22*) described the effect as an upshift from

[4] In fact, we cannot say which band shifts up and which shifts down, but for ease of reference we speak of the 1456 cm^{-1} moving to higher frequency. This arbitrary but reasonable choice minimizes the magnitude of both shifts.

1447 to 1464 cm^{-1} but did not comment on the contribution at 1456 cm^{-1}. Such a large, ^2H_2O-induced upshift would be unprecedented and hardly diagnostic of simple hydrogen bonding. In fact, we find that the 1447 cm^{-1} component is ^2H_2O sensitive but is probably downshifted by about 12 cm^{-1}, consistent with a strongly hydrogen bonded C═O group, so the basic conclusion of Breton and co-workers stands. However, the oversight of the 1456 cm^{-1} component weakens their proposed partitioning of C1 and C4 carbonyl vibrations to the modes of the main anion band. Furthermore, in neither study with site-specifically ^{13}C-labeled quinone (*18*, *19*) could a contribution of the C1═O vibration to the 1447 cm^{-1} band be ruled out. Thus, at the present time, it is still not clear how the potential energy of the two C═O vibrations is distributed, and the two peaks at 1447 and 1456 cm^{-1} may both contain C4═O and C1═O contributions. We suggest that these transitions decouple upon $^1H/^2H$ exchange and shift in opposite directions, as we observe.

The band or shoulder at 1482−1484 cm^{-1} is significantly affected by all three mutations and by $^1H/^2H$ exchange. However, following Brudler et al. (*19*), we ascribe most of the changes in this region to primary effects on an underlying negative band (quinone-associated), of unknown identity. This is present but much less apparent in the spectra of Breton and co-workers and is presumably somehow preparation- or sample-dependent. In our hands, it is seen in the double difference spectra between GaWT and M265 mutant RCs. In ^1H_2O, it shows as a negative band at 1485 cm^{-1} (Figure 5, side panel). In ^2H_2O, it is even more apparent—the negative band sharpens and upshifts to 1491 cm^{-1} and is seen as a very distinct negative peak in the GaWT-minus-mutant double difference spectra (Figure 5, main panel). Comparison of Figures 2, 3, and 5 indicates that the band is largest in wild type, smaller in M265IV, and essentially absent in the polar mutants. This allows the real magnitude of the 1482 cm^{-1} semiquinone band to become more apparent in the mutants, and it is seen as a distinct peak in M265IS and M265IT RCs. With this underlying activity, however, it is difficult to deduce what the effect of the mutations is on the 1482 cm^{-1} semiquinone band, but it is not evidently shifted in ^2H_2O, in agreement with earlier work and with the assignment of this peak to a C═C mode (*20*, *22*).

IR Responses of the Protein. Amide I and Amide II Regions. The light-induced formation of Q_A^- is expected to produce changes in the protein. Even if these do not involve specific side chain effects, significant spectral responses can arise through the sensitivity of the peptide bond to small changes in conformation. These are seen in two major regions of the IR spectrum: (i) the amide I band, between 1620 and 1680 cm^{-1}, which is associated with the C═O stretching mode, and (ii) the amide II band, between 1520 and 1570 cm^{-1}, which arises from a mixture of largely C−N stretch and N−H deformation modes. Much effort has been expended in trying to assign characteristic peptide amide frequencies to specific protein secondary structures, and some success has been achieved in the amide I region (*21*, *39*−*42*). Some identification can be made between α-helices, *β*-strands, and turns, but the distinctions are rarely clear-cut. The theoretical correlates for these assignments are the strength of the hydrogen bonds, dipole−dipole interactions, and the torsional angle of the peptide bond (*43*−*47*). The C═O stretching frequency is lowered by a stronger hydrogen bond and dipole−dipole alignment and raised by nonplanarity of the peptide bond, which affects the C═O bond order.

It is clear that reduction of Q_A induces significant responses in both amide I and amide II regions. The main features seen here, at 1676(+)/1670(−)/1659(+) cm^{-1} and 1564(+)/1556(−)/1543(+)/1531(−) cm^{-1}, have been observed in all FTIR studies of RCs, although the relative intensities are somewhat variable. The peak frequencies are almost the same in ^1H_2O and in ^2H_2O, with downshifts of no more than 1 cm^{-1}, but there are underlying changes that are apparent from the effects on the intensities around 1670 cm^{-1} and 1564/1556 cm^{-1}. ^1H_2O-minus-^2H_2O double difference spectra show a substantial increase in a negative peak at 1668 cm^{-1} and a positive peak at 1558 cm^{-1} in all strains, and a significant negative peak at 1614 cm^{-1} for all except M265IS, which has a small peak at 1608 cm^{-1}. Surprisingly, and as noted by Breton and Nabedryk (*22*), there is no indication of a corresponding band in the amide II′ region (around 1450 cm^{-1}) characteristic of deuterated peptides—the signals that are seen at 1456/1447 cm^{-1} seem to be associated with the semiquinone (*17*, *18*).

Three possibilities might be suggested for the signals at 1668(+) and 1558(−) cm^{-1} seen in the ^1H_2O-minus-^2H_2O double difference spectra. The simplest is an intensity shift between the amide I and the amide II modes. The frequencies are at the high end of both spectral regions and might indicate that the relevant peptide is in a turn motif, with strained $\phi-\psi$ angles and nonideal hydrogen bond geometries. A more specific suggestion, possibly also involving the 1614 cm^{-1} band, is a role for a primary amide, such as asparagine M258, which is hydrogen bonded to the peptide C═O of Ala^{M260}. The C═O and N−H modes of primary amides are very dependent on hydrogen bonding, and the N−H deformation of primary amides undergoes a massive shift upon deuteration, usually moving to below 1200 cm^{-1} (*37*), out of the range covered here. A third proposal could involve responses from arginine M267 and possibly glutamic acid M263, which form a salt bridge near the surface of the protein, at the membrane−water interface. Arginine is characterized by strong transitions near 1670 ($\upsilon_{as}(CN_3H_5^+)$) and 1615 cm^{-1} ($\upsilon_s(CN_3H_5^+)$), respectively, and the symmetric mode downshifts substantially to about 1575 cm^{-1} in ^2H_2O (*37*, *48*, *49*). Carboxylates absorb near 1560 cm^{-1} ($\upsilon_{as}(CO_2^-)$) and 1400 cm^{-1} ($\upsilon_s(CO_2^-)$), but both frequencies are only weakly responsive to ^2H_2O. Further studies are underway to explore these proposals.

The ^1H_2O-minus-^2H_2O and GaWT-minus-mutant double difference spectra reveal amide I and II responses that appear to be unique to the polar mutants—a bandshift contribution at about 1640(+)/1630(−) cm^{-1}, which shifts only slightly in ^2H_2O but changes significantly in amplitude (Figure 4), and new bandshifts at 1675(+)/1668(−) cm^{-1} and 1557(−)/1545(+) cm^{-1} (or possibly 1545(+)/1533(−) cm^{-1}) (see Figure 5 for spectra in ^2H_2O). It seems likely that these arise from effects of the hydrogen bonding interaction between the serine and the threonine OH and the backbone strand of residues M258−262.

The shoulder at 1256 cm^{-1} on the methoxy band would not normally warrant attention except for its small magnitude in GaWT, greatly exaggerated contribution in M265IS, and disappearance in ^2H_2O. From the ^1H_2O-minus-^2H_2O double

difference spectra, it seems that this signal arises from a bandshift at 1260(+)/1254(−) cm^{-1} in ^1H_2O, which probably moves to 1238(+)/1231(−) cm^{-1} in ^2H_2O. A possible identification is an amide III contribution, or the similar mixed CN/NH mode from tryptophan (e.g., Trp^{M252}), which is in a $\pi-\pi$ interaction with the quinone. It may be significant that the amplitude of the 1260(+)/1254(−) cm^{-1} feature is much larger in the serine mutant, as is the upshift in the anion band 1471(−)/1456(+) cm^{-1}.

Side Chain Contributions. Although interpretation of such complex spectra is hazardous, the double difference spectra between GaWT and all three M265 mutants show a small band at 1368 cm^{-1} that may warrant some comment. The Q_A^-/Q_A difference spectrum for wild type RCs shows two negative peaks in this region, and the peak at 1375 cm^{-1} has been assigned to the C5 methyl of ubiquinone (*18*). The second peak, at 1369 cm^{-1}, is missing in the M265 mutants. This is a good group frequency for the symmetrical deformation mode (δ_{sym}) of CH_3 and is even specifically characteristic of structures with two methyl groups present, as in isoleucine (*36*, *37*). We therefore suggest that it corresponds to the C_δ methyl of Ile^{M265}, which is in direct contact with the headgroup of Q_A.

CONCLUSIONS

The infrared spectra of three mutants at residue M265 in the Q_A binding site have been described in the context of a structural model for the mutations. Substitution of Ile^{M265} with the hydroxyl-bearing residues, serine and threonine, causes a large drop in the redox potential of Q_A. This is suggested to arise from hydrogen bonding of the OH to the peptide C═O of Thr^{M261}, which causes a displacement of the backbone strand that bears the hydrogen bond donor (Ala^{M260}) to the C1 carbonyl of Q_A, lengthening the hydrogen bond to the semiquinone state, Q_A^-, and thereby destabilizing it. The effects of this perturbation on the Q_A^-/Q_A IR difference spectrum are consistent with this interpretation. The neutral quinone spectrum is only slightly affected, with a small upshift in the C═O stretch frequency at 1601 cm^{-1}, assigned to the C4 carbonyl. The anion band, centered at ≈1460 cm^{-1} and characteristic of the semiquinone state, is substantially affected by all three residue substitutions. In the polar mutants, and correlated with the decrease in E_m of Q_A, the main peak shifts to lower frequency. In the valine mutant, in which the E_m of Q_A is unchanged, the band splits, but the average frequency is unaffected. The semiquinone anion IR spectrum is still rather poorly understood, but shifts in the spectrum in ^2H_2O suggest further refinements of the partitioning of the C1═O and C4═O vibrations to the resultant modes. The effects of these mutations, especially the ^2H_2O sensitivity of their semiquinone spectra, suggest that they will be useful in studies with ^{13}C-labeled quinones, to further define the nature of the semiquinone vibrations.

ACKNOWLEDGMENT

We are grateful to R. L. Schowen (U. Kansas) and J. Heberle (Jülich, Germany) for useful discussions of the effects of $^2H/^1H$ exchange on hydrogen bond strengths and on IR spectra, respectively, and to R. Pokkuluri and M. Schiffer (Argonne National Labs) for the coordinates of PDB file 1K6L prior to release.

REFERENCES

1. Shinkarev, V. P., and Wraight, C. A. (1993) in *The Photosynthetic Reaction Center* (Deisenhofer, J., and Norris, J. R., Eds.) pp 193−255, Academic Press, San Diego.
2. Okamura, M. Y., and Feher, G. (1995) in *Anoxygenic Photosynthetic Bacteria* (Blankenship, R., Madigan, M., and Bauer, C., Eds.) pp 577−593, Kluwer Academic Publishers, Dordrecht.
3. Deisenhofer, J., and Michel, H. (1989) *Science 245*, 1463−1473.
4. Feher, G., Allen, J. P., Okamura, M. Y., and Rees, D. C. (1989) *Nature 339*, 111−116.
5. Prince, R. C., Halbert, T. R., and Upton, T. H. (1988) in *Advances in Membrane Biochemistry and Bioenergetics* (Kim, C. H., Tedeschi, H., Diwan, J. J., and Salerno, J. C., Eds.) pp 469−478, Plenum Press, New York.
6. McComb, J. C., Stein, R. R., and Wraight, C. A. (1990) *Biochim. Biophys. Acta 1015*, 156−171.
7. Robinson, H. H., and Kahn, S. D. (1990) *J. Am. Chem. Soc. 112*, 4728−4731.
8. Burie, J.-R., Boullais, C., Nonella, M., Mioskowski, C., Nabedryk, E., and Breton, J. (1997) *J. Phys. Chem. B 101*, 6607−6617.
9. Coleman, W. J., Youvan, D. C., Aumier, W., Eberl, U., Volk, M., Lang, E., Siegl, J., Heckmann, R., Lersch, W., Ogrodnik, A., and Michel-Beyerle, M. E. (1990) in *Current Research in Photosynthesis* (Baltscheffsky, M., Ed.) pp 153−156, Kluwer Academic Publishers, Dordrecht.
10. Stilz, H. U., Finkele, U., Holzapfel, W., Lauterwasser, C., Zinth, W., and Oesterhelt, D. (1994) *Eur. J. Biochem. 223*, 233−242.
11. Takahashi, E., Warncke, K., and Wraight, C. A. (1998) in *Photosynthesis: Mechanisms and Effects* (Garab, G., Ed.) pp 853−856, Kluwer Academic Publishers, Dordrecht.
12. Takahashi, E., Wells, T. A., and Wraight, C. A. (2001) *Biochemistry 40*, 1020−1028.
13. Takahashi, E., Maróti, P., and Wraight, C. A. (1990) in *Current Research in Photosynthesis* (Baltscheffsky, M., Ed.) pp 169−172, Kluwer Academic Publishers, Dordrecht.
14. Takahashi, E., and Wraight, C. A. (1992) *Biochemistry 31*, 855−866.
15. Kunkel, T. A. (1985) *Proc. Natl. Acad. Sci. U.S.A. 82*, 488−492.
16. Breton, J., Nabedryk, E., Allen, J. P., and Williams, J. C. (1997) *Biochemistry 36*, 4515−4525.
17. Breton, J., Burie, J.-R., Berthomieu, C., Berger, G., and Nabedryk, E. (1994) *Biochemistry 33*, 4953−4965.
18. Breton, J., Boullais, C., Burie, J., Nabedryk, E., and Mioskowski, C. (1994) *Biochemistry 33*, 14378−14386.
19. Brudler, R., de Groot, H. J. M., van Liemt, W. B. S., Steggerda, W. F., Esmeijer, R., Gast, P., Hoff, A. J., Lugtenburg, J., and Gerwert, K. (1994) *EMBO J. 13*, 5523−5530.
20. Breton, J., and Nabedryk, E. (1996) *Biochim. Biophys. Acta 1275*, 84−90.
21. Arrondo, J. L. R., Muga, A., Castresana, J., and Goñi, F. M. (1993) *Prog. Biophys. Mol. Biol. 59*, 23−56.
22. Breton, J., and Nabedryk, E. (1995) in *Photosynthesis: From Light to Biosphere* (Mathis, P., Ed.) pp 395−400, Kluwer Academic Publishers, Dordrecht.
23. van Gunsteren, W. F., Billeter, S. R., Eising, A. A., Hünenberger, P. H., Krüger, P., Mark, A. E., Scott, W. R. P., and Tironi, I. G. (1996) *Biomolecular Simulation: The Gromos 96 Manual and User Guide*, BIOMOS b.v., University of Groningen, The Netherlands.
24. Guex, N., and Peitsch, M. C. (1997) *Electrophoresis 18*, 2714−2723.
25. Stowell, M. H. B., McPhillips, T. M., Rees, D. C., Soltis, S. M., Abresch, E., and Feher, G. (1997) *Science 276*, 812−816.
26. Ermler, U., Fritzsch, G., Buchanan, S. K., and Michel, H. (1994) *Curr. Biol. Structure 2*, 925−936.
27. Pokkuluri, P. R., Laible, P. D., Deng, Y.-L., Wong, T. N., Hanson, D. K., and Schiffer, M. (2002) *Biochemistry 41*, 5998−6007.
28. Gunner, M. R., Braun, B. S., Bruce, J. M., and Dutton, P. L. (1985) in *Antennas and Reaction Centers of Photosynthetic Bacteria: Structure, Interactions and Dynamics* (Michel-Beyerle, M. E., Ed.) pp 298−304, Springer-Verlag, Berlin.
29. Warncke, K., and Dutton, P. L. (1993) *Biochemistry 32*, 4769−4779.
30. Feher, G., Isaacson, R. A., Okamura, M. Y., and Lubitz, W. (1985) in *Antennas and Reaction Centers of Photosynthetic Bacteria−Structure, Interactions, and Dynamics* (Michel-Beyerle, M. E., Ed.) pp 174−189, Springer-Verlag, Berlin.

31. Bauscher, M., and Mäntele, W. (1992) *J. Phys. Chem. 96*, 11101−11108.
32. De Groot, H. J. M. (1995) in *Photosynthesis: from Light to Biosphere* (Mathis, P., Ed.) pp 401−406, Kluwer Academic Publishers, Dordrecht.
33. Paddock, M. L., Abresch, E. C., Isaacson, R. A., Lubitz, W., Okamura, M. Y., and Feher, G. (1999) *Biophys. J. 76*, A141.
34. Breton, J., Burie, J., Boullais, C., Berger, G., and Nabedryk, E. (1994) *Biochemistry 33*, 12405−12415.
35. Warncke, K., Gunner, M. R., Braun, B. S., Gu, L., Yu, C.-A., Bruce, J. M., and Dutton, P. L. (1994) *Biochemistry 33*, 7830−7841.
36. Bellamy, L. J. (1975) *The Infrared Spectra of Complex Molecules*, 3rd ed., Chapman and Hall, London, New York.
37. Barth, A. (2001) *Prog. Biophysics Mol. Biol. 74*, 141−173.
38. Sheppard, N. (1955) *Trans. Faraday Soc. 51*, 1465−1468.
39. Krimm, S., and Bandekar, J. (1986) *Adv. Protein Chem. 38*, 181−364.
40. Dong, A., Huang, P., and Caughey, W. S. (1990) *Biochemistry 29*, 3303−3308.
41. Bandekar, J. (1992) *Biochim. Biophys. Acta 1120*, 123−143.
42. Jackson, M., and Mantsch, H. H. (1995) *Critical Rev. Biochem. Mol. Biol. 30*, 95−120.
43. Krimm, S. (1955) *J. Chem. Phys. 23*, 1371−1372.
44. Krimm, S. (1962) *J. Mol. Biol. 4*, 528−540.
45. Cannon, C. G. (1956) *J. Chem. Phys. 24*, 491−492.
46. Moore, W. H., and Krimm, S. (1975) *Proc. Natl. Acad. Sci. U.S.A. 72*, 4933−4935.
47. Jackson, M., and Mantsch, H. H. (1991) *Can. J. Chem. 69*, 1639−1642.
48. Chirgadze, Y. N., Fedorov, O. V., and Trushina, N. P. (1975) *Biopolymers 14*, 679−694.
49. Venyaminov, S. Y., and Kalnin, N. N. (1990) *Biopolymers 30*, 1243−1257.

BI026958J